Engineering with Computers (2022) 38 (Suppl 4):S2663–S2680
https://doi.org/10.1007/s00366-021-01420-9

ORIGINAL ARTICLE

An intelligent fuzzy-based hybrid metaheuristic algorithm for analysis the strength, energy and cost optimization of building material in construction management

Song Ronghui[1] · **Ni Liangrong**[2]

Received: 12 January 2021 / Accepted: 5 May 2021 / Published online: 22 May 2021

Abstract
Optimization is one of the oldest sciences or practices. Since the beginning of mankind, people strived for perfection when it came to their creations, products, gains, or self-improvement. Extension of activities and their cost, time, and resource limitations have caused researchers to pay their attention to optimizing the activities in construction management engineering. Rapid development in optimization techniques to solve related problems in structural design can be achieved accordingly. In this paper, meta-heuristic algorithms used for strength, energy, and cost optimization of building material in construction management. The novel meta-heuristic algorithm can be used for electricity cost and peak load alleviation with the minimum user waiting time. The proposed model is implemented in a smart building in terms of electricity cost estimation for both a single smart home and a smart building. The results demonstrate the effectiveness of our proposed scheme for single and multiple smart homes in terms of strength, energy, and cost optimization of building material in construction management engineering. This study has used the artificial intelligence (AI) model as particle swarm optimization (PSO) model to calculate the accurate and material-specific energy of three commonly used building materials as fly ash, copper slag, and phospo-gypsum. Two regression models as root mean square (RMSE) and coefficient of determination (R^2) were used to calculate the results. Following the results of (R^2) and RMSE, PSO has shown its higher performance in predicting the strength, energy, and cost of building materials besides revealing a significant and positive correlation among them.

Keywords Hybrid metaheuristic algorithm · Particle swarm optimization · Cost optimization · Construction management · Artificial intelligence · Building material

1 Introduction

Embodied energy is the energy consumed by all of the processes associated with the production of a building, from the mining and processing of natural resources to manufacturing, transport and product delivery [1–12]. Analysis across Australia and elsewhere found that the building's energy is a large part of the annual intake of working energy [13]. It ranges from 10 average homes to more than 30 offices (CSIRO[1] 2000). Increasing the energy efficiency in buildings such as houses typically entails more energy and more ratio. However, experience in the trade sector has shown that the effect of energy on the overall building footprint is increasing as energy efficiency in buildings increases because of the ratios between energy and total energy usage [14–17]. CSIRO analysis indicates that building requires an average of about 1000 GJ of energy incorporated in building materials, which corresponds to the normal use of operating resources for around 15 years [18]. This is more than 10% of the electricity used in a house that lasts 100 years. The use of energy figures in construction should be careful. It is also possible to recycle certain products and to reduce the effects during their life cycle, e.g. aluminium from a recycled source contains less than 100% of the energy of the aluminium produced from raw materials [18–24]. In Canada

✉ Song Ronghui
42763610@qq.com

[1] Zhejiang Tongji Vocational College of Science and Technology, Zhejiang 311231, China

[2] China United Engineering Corporation Limited, Hangzhou 310052, China

[1] Commonwealth Scientific and Industrial Research Organization.

Fig. 1 Using cork in construction materials mixed with concrete to reduce the weight and cost of materials

for example, only non-renewables in embodied energy sources were considered. Thus, it can be shown that many considerations must be weighed when evaluating potential areas in which commercial buildings can reduce their energy levels by retrofitting [13]. Researchers were interested in the interactions between building materials, construction practices, also their environmental effects have researched energy in building materials. Figure 1 shows the effective use of cork as a light weight material during a concrete mixed processing.

For many decades, low-energy materials, such as concrete, bricks or wood are highly used, however, materials with more energy level, such as stainless steel are rarely used [25–39]. Around 2003 and 2030, global energy consumption is predicted to increase to 71%. At the moment, great energy use is dependent on fossil fuels and it is unclear if such a demand trend will be followed environmentally sustainable considering significant developments in renewable energy technologies. Therefore, it is recommended that only the order-of-magnitude enhancements to energy quality should be achieved, particularly as the ratio of resources delivered to energy consumed to prevent a dramatic decrease in agreed living standards [40–46]. Energy is one of the main drivers in all countries for economic growth and social development [47] as the increasing reason of CO_2 energy emissions in past 20 years [40, 48, 49]. Construction projects account for 38% of the world's overall energy usage [50]. More responsibility for the pollution issue needs to be taken by the construction sector. Energy is used at various levels in each phase of the construction life cycle. Because of its environmental positive elements, energy-efficient materials will sustain constructions both economically and ecologically. In comparison, energy-reducing products cause less harmful emissions, also the waste from building materials is being decreased. They also contribute to the development of comfort in indoors due to their different thermal features, such as heat conservation and heat retention [51]. Finally, it is because of these considerations that choosing of the best material at the outset of design process must take account of energy-efficient properties along with several requirements for the environmental features. As the population and urbanization rise, energy demand is growing rapidly.

Depending on the environment, the form and degree of construction energy differ from region to region [52]. Construction consumes 38% of the world's energy annually [50]. The energy usage of buildings and their potential detrimental effects on the atmosphere are becoming extremely severe. Several new studies have sought to classify energy efficiency, environmental impacts of housing and construction materials. The use of overall energy for the given sample room was explored by [40, 53]. The paper focuses on comparing two structures of bricks made from fire clay and structures made from ash blocks. While ash blocks are three times more expensive than flames, their scale, total use of electricity, and their ultimately total construction costs (due to their light weight and isolation) have been considerably reduced [54]. The embodied energy of various construction materials was studied (conventional building materials and alternative building materials). These researches involved the efficiency of few operating energy materials. In comparison to traditional construction materials, it is seen that alternative building materials and systems have minimized and/or equivalent impacts on life cycle costs [55–60]. Furthermore, stability and instability analysis of the composite, conceit, and smart material and structures take the attentions of researchers in different filed of engendering [61–65].

In recent years, in addition to the experimental and numerical techniques, artificial intelligence (AI) algorithms have been developed and employed in various fields, especially civil engineering [66–70]. In fact, AI is able to accurately optimize and predict the experimental data. Researchers have developed several sub-sets of AI algorithms such as ANFIS, PSO, machine learning, and hybrid algorithms-like PSO-ELM, ANFIS-PSO [71–75]. The advantages of AI models compared to experimental methods are high accuracy and cost-effectiveness. Also, they require lower time to process the data than other numerical approaches [76–80] (Figs. 2 and 3).

2 The related literature

Regarding the energy efficiency of building materials, energy needs to be used less quickly in each step of the life cycle, particularly in the overall energy use of construction process and the proportion of energy utilized for the production and transport of building materials [81–84]. Therefore, in all phases, the preferential of building materials, by the production, transportation, use and destruction of their raw material offers energy efficiency to construction [36, 40, 51,

Fig. 2 Frame of light-weight construction processing by the integration of cork and wood

Fig. 3 Using cork palates in a building to reduce the energy losing and noise

Fig. 4 Using the tree trunk in a processing of concrete mixed materials for energy, lightweight and cost issues

85–89]. The selection of a building material can influence the energy usage of that building over the various phases of its life cycle and can have opposite consequences. Given that properties like a high level of insulation can provide relative efficiency savings in operating energy along with greater embodied energy costs. The balance of the exterior building system and envelope (roof, board, walls and windows) seems to represent the highest part of its energy [50]. In the case of building materials, the proportion of energy consumed to its overall energy consumption is calculated at 50 years, but ranges from 6 to 20% according to the method and environment of construction [90, 91]. Energy performance requirements for building materials can be categorized in two categories: directly and indirectly effective criteria [92, 93].

The US building industry uses more than 48% annual electricity in construction and service, which contributes to substantial emissions of carbon dioxide into the air. This electricity is often incorporated and working energy is used over the life span of a structure [94] Building uses operating energy in hot water supply, lighting, space conditioning and powering building appliances. Studies have proposed using a systemically based approach to a life cycle energy assessment in a building to significantly minimize this carbon footprint and extensive energy [95]. A systematic energy evaluation is used for the use of energy, as well as for the use, regeneration, and reuse of energy by means of green energy technologies and recycler efforts. The main focus of research activities has been on operational energy optimization with new innovative building envelope and machinery materials [96–101]. Then, the electricity in building is increased because much of this specialized products or machinery are made by energy-intensive manufacturing methods [83, 102–106]. In a building, the energy is used directly through construction by the use of construction materials. The construction, manufacturing, logistics, administration, and related processes include a number of on-site and off-site energy sources. Furthermore, any building material includes energy during its production and distribution. The overall energy of a building during its life cycle consists of initial (IEE), recurrent (REE) and demolition embodied energy (DEE) [107, 108]. IEA involves both resources used directly and indirectly (e.g. during transport and construction) to build a construction. The completeness of an energy measurement is based on the system boundary covered. There are few methods for measuring the embodied energy, such as IO-based, process-based and hybrid methods. Each process uses various data source types and covers differing systems boundary dimensions [109–113]. The findings are not identical because of these variations. In addition, any process has data quality and device integrity limitations. For example, a process-based approach uses real data from manufacturers' sources, which are known to be robust in their reliability and representation [109, 114, 115]. This approach has insufficient findings,

(a)

(b)

Fig. 5 Construction of building based on the tree trunk and cork

because it lacks inputs from which data cannot be available [102, 116–119] (Figs. 4 and 5).

2.1 Embodied energy calculation: energy and cost relationship

Studies have shown that despite efforts at defining a standard system boundary and deriving an appropriate method of calculating embodied energy, they are reliable, consistent, and consistent. Few materials are used in construction materials to reduce the cost and energy losing, say cork, trunk of tree, coffee husks, newspaper woods, mycelium, recycled diapers, plastic bricks, polyurethane plant based foam fly ash, silica fume and etc. On the other hand, an energy analysis is costly and time-consuming and is dependent on many assumptions [114]. Furthermore, energy research is not well incorporated into the existing design and building practices, so decisions are mostly taken only on the basis of cost. Studies have found a relationship between consumption of embodied energy and cost. Stern and Cleveland [120] agreed that economic growth means a proportional growth in energy usages. Also, at the project stage, Langston et al. [121] found a clear and optimistic connection between the costs and the energy in a house [122] (Fig. 6).

Some researchers investigated the connection of energy consumption and cost optimization in a study of three low-rise apartments in Indonesia. Since the buildings consisted of hollow blocks in the interior and outside walls, two other light-weight concrete and brick walls alternatives were also studied (Table 1).

2.2 Problem statement

Due to lack of total, precise, and detailed energy data, the measurement of energy is complicated, then this study employed PSO to accurately calculate the strength, energy and cost optimization of building materials [123–132]. The aim of this paper is to accurately predict the cost and energy reduction in using alternative wall material for construction, through detailed analysis in a residential building [4, 133–141] (Figs.7, 8 and 9).

3 Methodology

3.1 Statistical data

150 data were originally extracted. The current study has investigated the strength, energy and cost optimization of materials in construction building using PSO. The model was developed and the results were analyzed by regression indicators.

3.2 Particle Swarm Optimization (PSO)

PSO as an optimization algorithm is determined in six phases [142–148]:

1. A group of random potential resolution is determined as the searching space. It is assumed that N is the number of particles and D is the dimensions of searching space. Both are used as the random "position" (X_i^k) and "velocity" (vi^k) of ith particle at iteration k as Eqs. (1) and (2).

$$v_i^k(t+1) = wv_i^k(t) + C_1 \cdot \text{rand}()\left(p_i^k(t) - X_i^k(t)\right) + C_2 \cdot \text{rand}()\left(g_i^k(t) - x_i^K(t)\right), \tag{1}$$

$$x_i^K(t+1) = x_i^K(t) + v_i^k(t+1) 1 \le i \le N, \quad 1 \le k \le D, \tag{2}$$

w is the iteration weight; rand ()" is a constant value in 0, 1 interval while set randomly; C_1 and C_2 is the different acceleration coefficients; g_i^k is the the global best

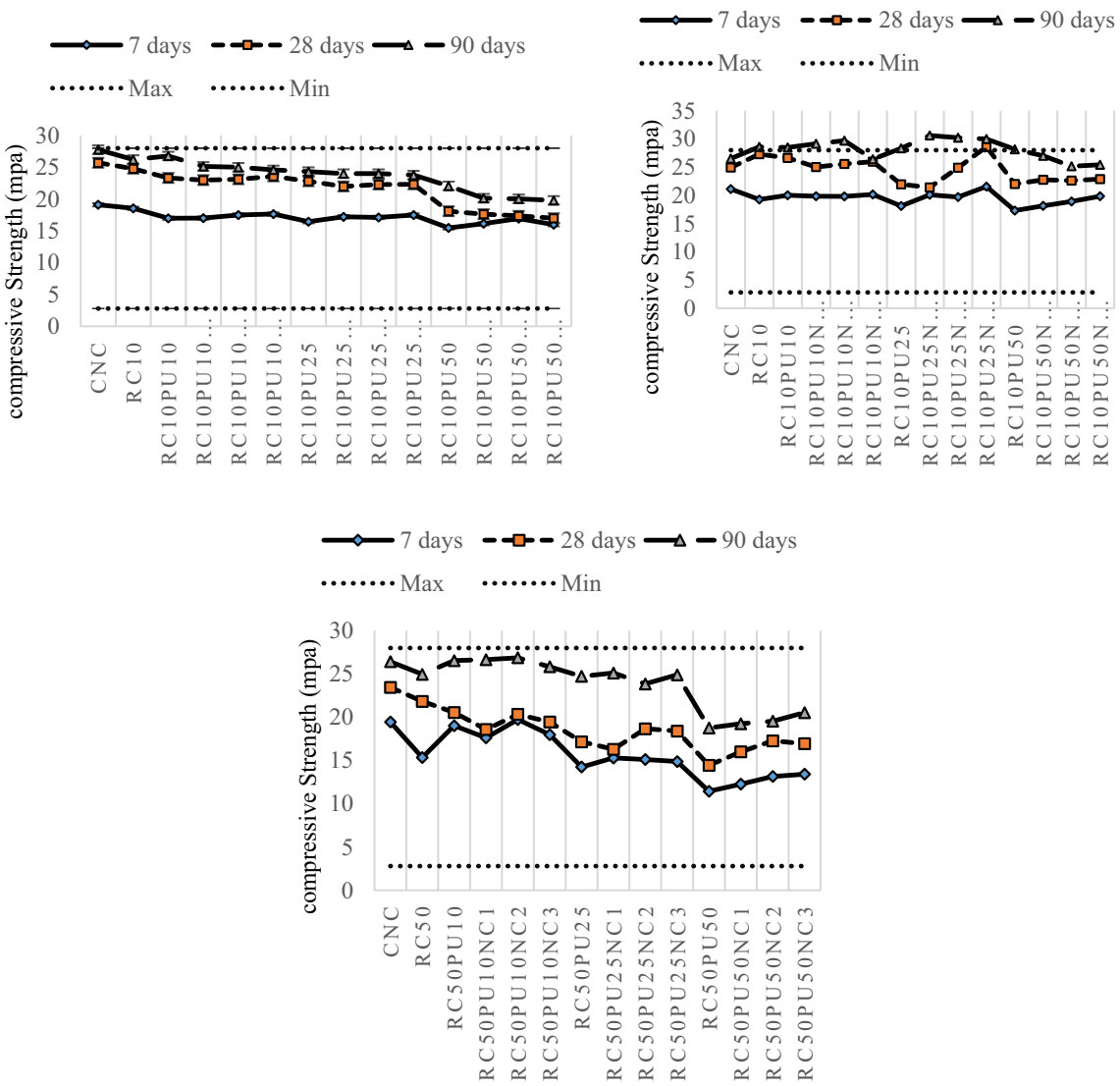

Fig. 6 The strength diagram of concrete while adding light-weight aggregates

position found in group; p_i^k is the the best position of ith particle in a search phase.

2. Evaluate the fitness of each particle in the swarm
3. Compare the fitness of each particle to its prior best-obtained fitness p_i^k in each iteration. If the current variable is better than p_i^k, then p_i^k is selected as the current variable and the p_i^k positon as the current position in d-dimensional space.
4. Compare the p_i^k of particles with one another and updating the swarm global best position with the most fitness g_i^k [149].
5. The velocity of each particle is changed (accelerated) towards its p_i^k and g_i^k. This acceleration is weighted by a random term. A new location in the solution space is computed for each particle by adding a new velocity variable to each component of the particle's position vector.
6. Repeat steps (2)–(5) until convergence is gained on the basis of proper criteria [150] (Figs. 10, 11, 12 and 13).

Table 1 Concrete mix proportions of silica fume and fly ash as light aggregates to concrete

Mix code	W/C[1]	B/C[2]	Water (kg/m^3)	Cement (kg/m^3)	Bentonite (kg/m^3)	sand 0–4.75 mm (kg/m^3)	Gravel 4.75–9.5 mm (kg/m^3)	Gravel 9.5–19 mm (kg/m^3)
A1	2.3	0.2	400	119	24	620	280	475
A2	2.2	0.2	400	125	29	620	280	475
A3	2.7	0.2	400	133	56	620	280	475
A4	2.1	0.2	400	142	35	620	280	475
A5	2.0	0.2	400	200	40	620	280	475
B1	3.0	0.3	400	133	40	620	280	475
B2	2.8	0.3	400	1413	43	620	280	475
B3	2.6	0.3	400	154	46	620	280	475
B4	2.4	0.3	400	167	35	620	280	475
B5	2.2	0.3	400	182	55	620	280	475
B6	2.0	0.3	400	200	60	620	280	475
C1	3.0	0.35	400	133	23	620	280	475
C2	2.8	0.36	400	143	50	620	280	475
C3	2.6	0.35	400	154	54	620	280	475
C4	2.4	0.32	400	167	55	620	280	475
C5	2.7	0.35	400	182	64	620	280	475
C6	2	0	400	200	67	620	280	475

Mix water (kg/m^3); cement (kg/m^3); coarse aggregate (kg/m^3); fine aggregate (kg/m^3) SP* (kg/m^3)

3.3 Equations of heat transferring

In this study, for analyzing the energy of composite, two equations are used. Considering the local equations, the two equations could show the transient heat exchange between the PCM and metal foam as follows:

Energy equation for metal foam:

$$(1-\varepsilon)\rho_s C_s \frac{\partial T_s}{\partial t} = \lambda_{se}\nabla^2 T_s + hA\left(T_p - T_s\right), \tag{3}$$

Energy equation for phase change material:

$$\varepsilon\rho_p C_p \frac{\partial T_s}{\partial t} + \varepsilon\rho_p C_p (U\cdot\nabla)T_p = \lambda_{pe}\nabla^2 T_p + hA\left(T_s - T_p\right) - \varepsilon\rho_p L\frac{\partial\beta}{\partial t}, \tag{4}$$

$$h = \frac{\lambda_p}{d_f}\left[1 + \frac{4(1-\varepsilon)}{\varepsilon} + 0.5(1-\varepsilon)^{0.5}\mathrm{Re}^{0.6}\,\mathrm{Pr}^{1/3}\right], \tag{5}$$

$$A = \begin{cases} 694.57\ln(1-\varepsilon) + 3579.99 & \mathrm{PPI} = 10 \\ 442.2\ln(1-\varepsilon) + 2378.62 & \mathrm{PPI} = 20 \\ 694.57\ln(1-\varepsilon) + 3579.99 & \mathrm{PPI} = 40 \end{cases}, \tag{6}$$

$$0 \le X \le 100, \quad y = 0, \quad \frac{\partial T}{\partial y} = 0;$$

$$0 \le X \le 100, \quad y = 300, \quad \frac{\partial T}{\partial y} = 0;$$

$$E(t) = E_{\mathrm{PCM}}(t) + E_{\mathrm{foam}}(t) + E_{\mathrm{fin}}(t), \tag{7}$$

$$E_{\mathrm{PCM}}(t) = \begin{cases} m_{\mathrm{PCM}}C_{\mathrm{s,PCM}}\left(T_{\mathrm{PCM}}(t) - T_0\right) T \le T_m \\ m_{\mathrm{PCM}}C_{\mathrm{l,PCM}}\left(T_{\mathrm{PCM}}(t) - T_m\right) \\ +m_{\mathrm{PCM}}C_{\mathrm{s,PCM}}\left(T_m - T_0\right) + m_{\mathrm{MPC}}LT > T_m \end{cases}, \tag{8}$$

$$E_{\mathrm{foam}} = m_{\mathrm{foam}}C_{\mathrm{al}}\left(T_{\mathrm{foam}} - T_0\right),$$

$$E_{\mathrm{fin}} = m_{\mathrm{fin}}C_{\mathrm{al}}\left(T_{\mathrm{fin}} - T_0\right),$$

$$P = \frac{E\left(t_{\mathrm{total}}\right)}{t_{\mathrm{total}}},$$

Initial condition : $0 \le X \le 100, \quad 0 \le y \le 300, \quad T_s = T_p = T_{\mathrm{fin}} = 323$ K,

Boundary conditions : $X = 0, \quad 0 \le y \le 300, \quad T_p = T_s = T_{\mathrm{fin}} = 351$ K,

(a)

(b)

(c)

Fig. 7 The installing of wooden construction parts for a building built from cork and wood

$$\text{Continuity equation}: \nabla \cdot U = 0,$$

$$\text{Momentum equation}: \frac{\partial U}{\partial t} + \frac{1}{\varepsilon}(U \cdot \nabla)U = \frac{\mu}{\rho}\nabla^2 U - \frac{\varepsilon}{\rho}\nabla P + F + S, \tag{9}$$

U is the velocity field of liquid paraffin; ρ is the density; ε is the porosity of foam; μ is the viscosity of the paraffin; F is the source term of resistance and driving force of flow expressed as

$$F = -\frac{\varepsilon}{\rho}\frac{\mu}{K}U + \varepsilon g \gamma \left(T - T_0\right), \tag{10}$$

K is the permeability; γ is the thermal expansion factor.

The value of K is gained through the following equations [24]:

$$K = 0.00073(1-\varepsilon)^{-0.224}\left(\frac{d_\mathrm{f}}{d_\mathrm{p}}\right)^{-1.11} d_\mathrm{p}^2, \tag{11}$$

$$\frac{d_\mathrm{f}}{d_\mathrm{p}} = 1.18\sqrt{\frac{1-\varepsilon}{3\pi}},$$

$$S_x = \mathrm{Au}_x,$$

$$S_y = \mathrm{Au}_y,$$

$$A = -C\frac{(1-\gamma)^2}{\gamma^3 + \varepsilon},$$

d_p is the diameter of pore; d_f is the diameter of the ligament.

The addition of the source term S in Eq. (9) is to compute the flow velocity in the mushy zone as

$$s = \frac{C\left(1-\beta^2\right)}{\alpha + \beta^3}, \tag{12}$$

$$\frac{\partial \rho}{\partial t} + \frac{\partial\left(\rho u_x\right)}{\partial x} + \frac{\partial\left(\rho u_y\right)}{\partial y} = 0,$$

$$\frac{\partial\left(\rho u_x\right)}{\partial t} + \nabla\left(\rho u_x \vec{u}\right) = -\frac{\partial \rho}{\partial x} + \nabla\left(\mu \nabla u_x\right) + S_x,$$

$$\frac{\partial\left(\rho u_y\right)}{\partial t} + \nabla\left(\rho u_y \vec{u}\right) = -\frac{\partial \rho}{\partial x} + \nabla\left(\mu \nabla u_y\right) + S_x + S_b,$$

α is a constant; C is the consecutive number for the mushy zone; the value is fixed at 10^6; β is the liquid fraction.

It could be determined by Eq. (11):

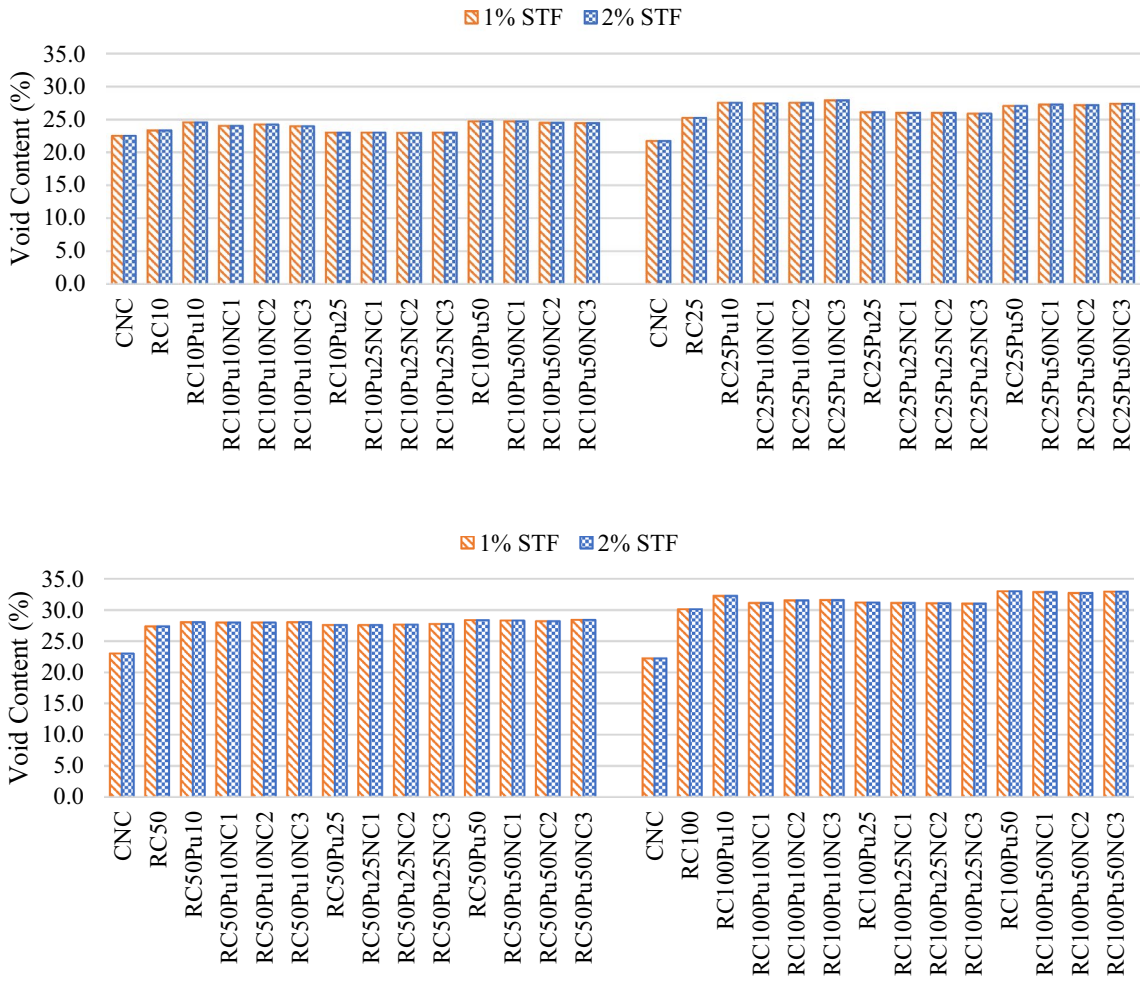

Fig. 8 The strength content of concrete while adding light-weight aggregates as cork and wood

Fig. 9 Molding the mixture of fly ash and cement

$$\beta = \begin{cases} 0 & T_p < T_{m1} \\ \left(T_p - T_{m1}\right)/\left(T_{m2} - T_{m1}\right) & T_{m1} \le T_p < T_{m2} \\ 1 & T_p \ge T_{m2} \end{cases} \tag{13}$$

$$0 \le X \le 300, \quad y = 100, \quad \frac{\partial T}{\partial x} = 0;$$

$$\gamma = \begin{cases} 0 & T < T_{\text{solidus}} \\ \frac{T - T_{\text{solidus}}}{T_{\text{liquidus}} - T_{\text{solidus}}} & T_{\text{solidus}} < T < T_{\text{liquidus}} \\ 1 & T > T_{\text{liquidus}} \end{cases} \tag{14}$$

$$\text{At outlet}, \frac{\partial T_f}{\partial y} = 0, \quad \frac{\partial u_y}{\partial y} = 0, \quad t > 0. \tag{15}$$

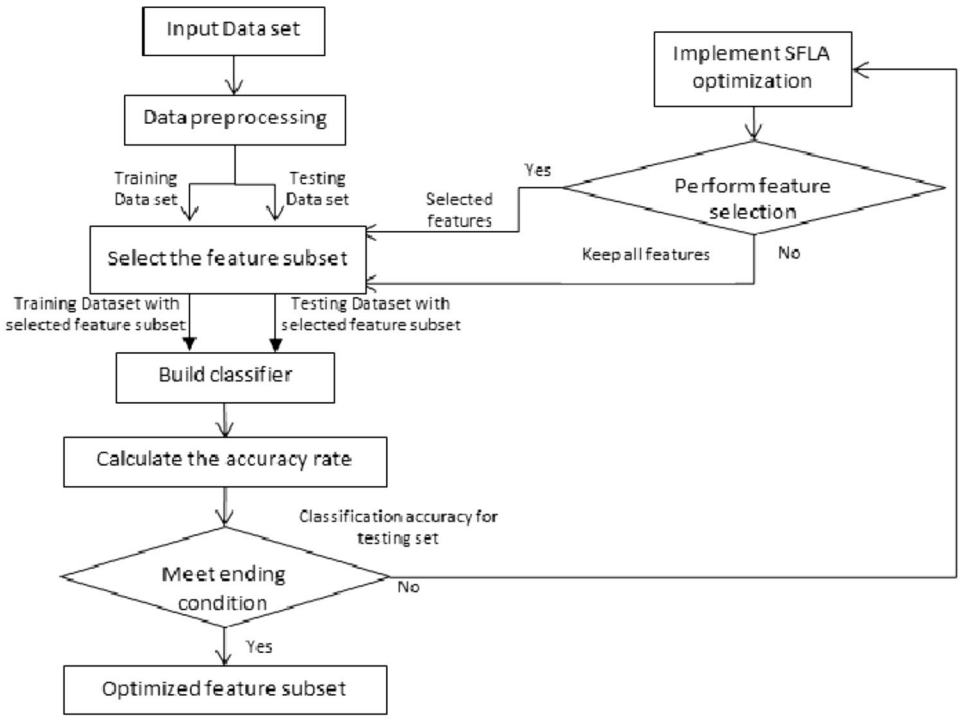

Fig. 10 PSO architecture

The wall of the heat storage tank is adiabatic, and the boundary condition is presented below

$$\frac{\partial T_f}{\partial x} = 0, \frac{\partial T_y}{\partial y} = 0, u_x = u_y = 0, \quad t > 0.$$

4 Result and discussion

4.1 Model performance indicators

According to the data derived from the literature, 30% of data is used in testing phase, while 70% is randomly assigned for training part. For comparing the results of PSO, statistical model performance indicators of determination coefficient (R^2) and root mean square (RMSE) were used.

$$R^2 = \frac{\left[\sum_{i=1}^{N}\left(O_i - \overline{O}\right)\cdot\left(P_i - \overline{P}\right)\right]^2}{\sum_{i=1}^{N}\left(O_i - \overline{O}\right)\cdot\sum_{i=1}^{N}\left(P_i - \overline{P}\right)}, \tag{16}$$

$$\mathrm{RMSE} = \sqrt{\sum_{i=1}^{N}\frac{1}{N}\left(O_i - P_i\right)^2}, \tag{17}$$

P is the predicted values; $\overline{P}$ is the predicted values; O is the observed values; O_i is the observed values in sample i; $\overline{O}$ is the mean of observed variables; N is the number of training or testing samples; P_i is the predicted values in sample i.

Note: R^2 of 1, and RMSE of 0 are the ideal form in a predictive model (Tables 2 and 3) (Fig. 14).

4.2 Data preparation

4.2.1 Data distribution pattern

In this study, PSO was used to accurately measure the embodied strength, energy and cost optimization of materials in construction building. Figures 15, 16, 17, and 18 showed the developing of the model and its diagrams. Figure 15 shows the results of PSO for the observed date (horizental axix) and predicted data (vertical) in determining the energy and cost optimization of materials in test phase. Accordingly, in Fig. 15, the observed data distribution is between − 1 to 1, also the distribution of predicted values is from − 1 to 1. The blue dots are almost over the black bold line, meaning that there is a good correlation between the predicted and obsrved values, showing the accuracy of PSO model in determimng the strength, energy and cost optimization of materials.

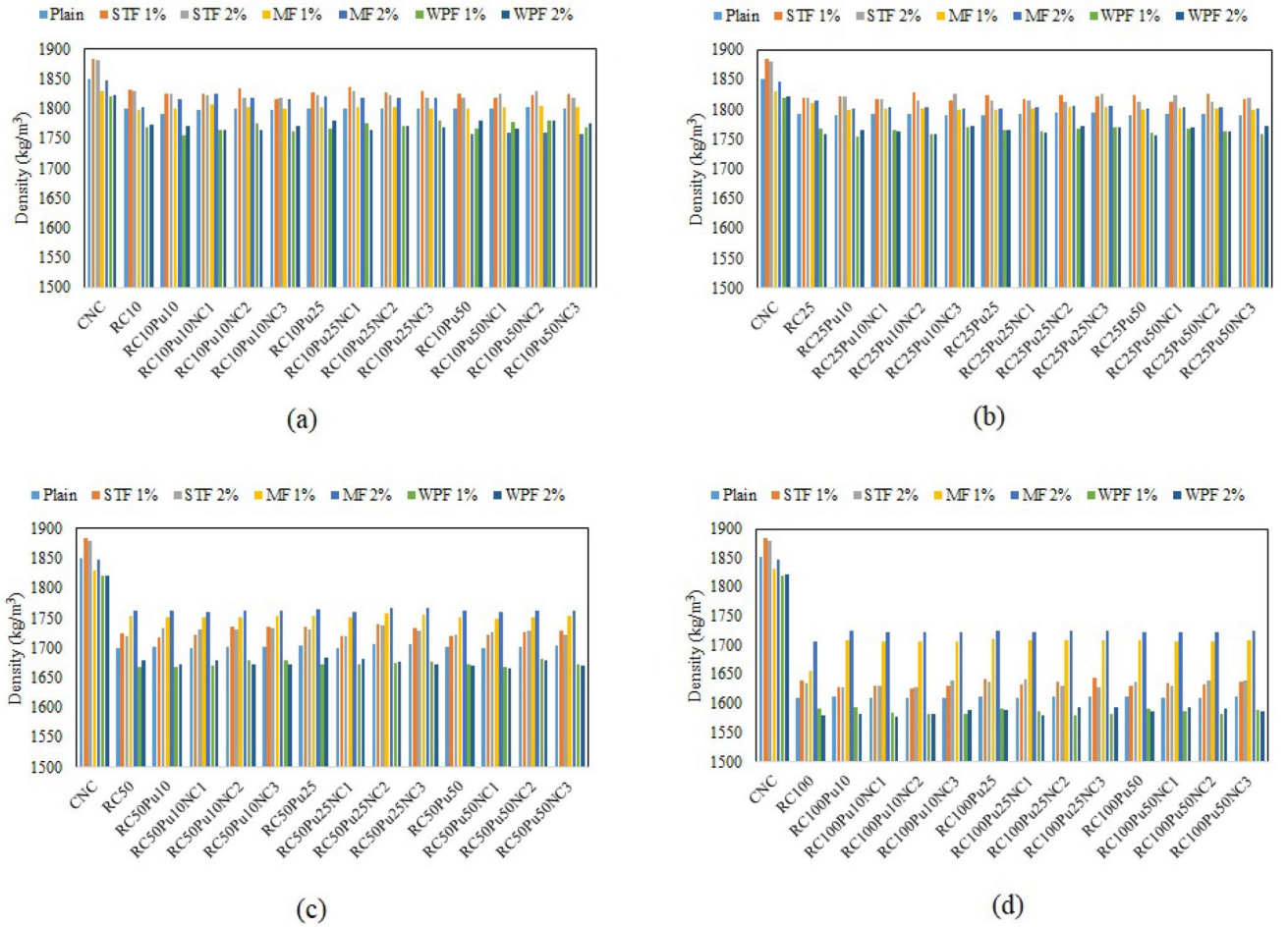

Fig. 11 Density plot of aggregate wile added to building material (brick) **a** lateral load test phase, **b** lateral load train phase, **c** compressive strength test phase, **d** compressive strength train phase

Fig. 12 Molding the mixture of fly ash and cement to produce light-weight bricks

Figure 16 shows the error distribution in PSO model in test phase. In Fig. 16, the horizontal axis is the error distance from − 2 to 1 and the vertical axis is the number of data distance. Also, the variance of value (σ) is 0.328 while the mean of value (μ) is − 0.113 in test phase. According to this diagram, the highest error was seen in 0.01 with 3 data and the lowest error was occurred in − 1 and 1 with roughly 1 data.

In Fig. 17 (observed error values), the horizontal axis is the number of data from 0 to 15 for PSO. The vertical axis is the errors value for this model.

In Fig. 18, the horizontal axis indicates the observed values of testing samples and the vertical line shows the predicted values. In this diagram, the blue line shows 100% alignment between the predicted and observed values (Ideal

(a)

(b)

Fig. 13 The molding process of production of fly ash bricks

form), while in this study, the radial lines have 15% differential from the black line (Fig. 18). Any overlap between these two lines means that our model reaches its ideal form with the least error percentages and high accuracy, however, it is not the case in our research (very less discrepancy). Then, PSO could show better performance in the analysis of the objective of this study. Comparing the R^2 of PSO as 0.9867, the results have shown that the R^2 value in PSO is nearer to 1 than, showing the best performance of PSO (Table 4) in this study. On the whole, because of the less difference between the predicted values and observed values, PSO has shown its best performance in predicting the strength, energy and cost optimization ofmaterials (Fig. 19).

Going through Table 4, the corresponding values of RMSE and R^2 could define the properness of the model. Obviously, the best RMSE value is the lowest one near to 0. In this study, the RMSE of PSO is 0.9606, also, the R^2 value in PSO is 0.9867. Comparing the R^2 values, the nearest value to 1 is considered as the best performance. Therefore, PSO could show better performance in terms of the objective of this study and proved itself as a satisfactory method to determine the energy and cost optimization of materials in construction management.

Figure 20 shows the best cost diagram. Regarding PSO, the weight of each neuron is changed to develop the model. In diagram 19, the vertical axis is cost and the horizontal axis is the number or iterations that were ordered to develop itself (90 times) to find its better performance. So, when the decreasing of cost reached to a stable case, it was stopped. It means that in our diagram, the cost was decreased at 10 iterations and was continued up to 90 iterations to find its stability. After 90 iterations, the running is stopped due to adequate stability of cost line. This diagram showed the drastically decline of cost while using non-conventional construction materials (Fig. 21).

5 Conclusion

Construction materials make up about 60–70% of the overall construction costs. It would not be necessary to minimize the use of traditional materials; thus the net construction expense of a house will be cut off by the new approach of low cost materials. When recycled and

Table 2 Assembly embodied energy, reduced embodied energy, and renewable energy of concrete slab, concrete tile and timber frame and steel sheets

Material	Original embodied energy mJ/kg	Reduced embodied energy in mining and construction per kg/MJ	Renewable energy used in mining and construction per kg/MJ	Optimum embodied energy mJ/kg
Elevated timber floor	293	567	345	345
110 mm concrete slab on ground	645	372	436	745
Roofs				
Timber frame, concrete tiles, plasterboard ceiling	251	346	845	453
Timber frame, steel sheets, plasterboard ceiling	330	563	452	345

Table 3 Assembly embodied energy, reduced embodied energy, and renewable energy of AAC block wall, steel frame and clay

Material	Original embodied energy mJ/kg	Reduced embodied energy in mining and construction per kg/MJ	Renewable energy used in mining and construction per kg/MJ	Optimum embodied energy mJ/kg
Single skin AAC block wall	440	789	678	788
Steel frame, compressed fibre cement clad wall	385	686	455	673
Cavity clay brick wall	860	765	300	573

Fig. 14 Light weight fly ash bricks to save energy and cost reduction

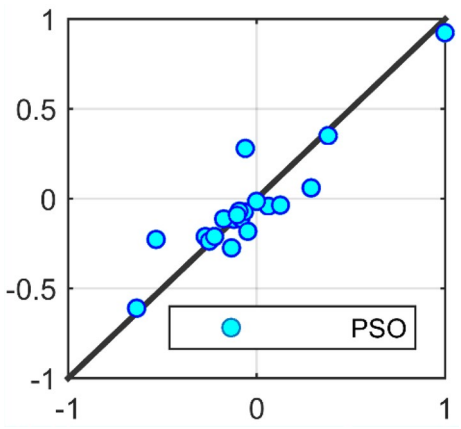

Fig. 15 AI results for energy and cost optimization values in PSO (test data). H axis = observed energy and cost optimization values. *V* axis = predicted energy and cost optimization values

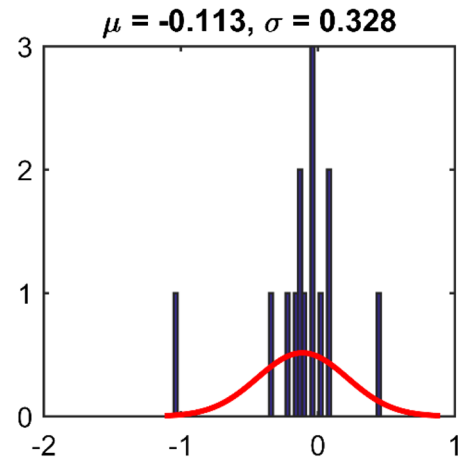

Fig. 16 Error distribution for PSO in test phase

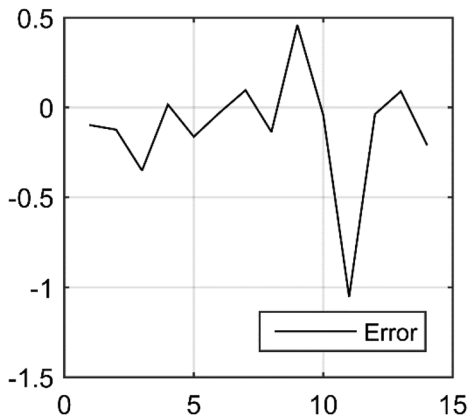

Fig. 17 Observed error values for PSO (test phase)

reused as construction materials, industrial waste not only tends to solve recycling challenges, but also conserves renewable resources, decreases energy consumption and reduces greenhouse gas emissions. When used as sand and coarse aggregate complements in the manufacturing

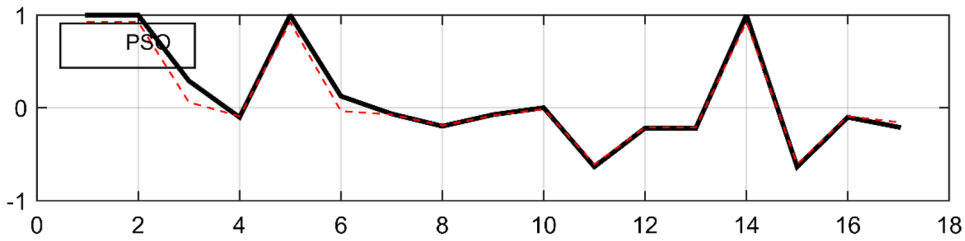

Fig. 18 The strength, energy and cost optimization of materials in construction management in PSO (test data)

Table 4 The training and testing phase results PSO

AI model	Training phase		Testing phase	
	RMSE	R^2	RMSE	R^2
PSO	0.9767	0.9899	0.9606	0.9867

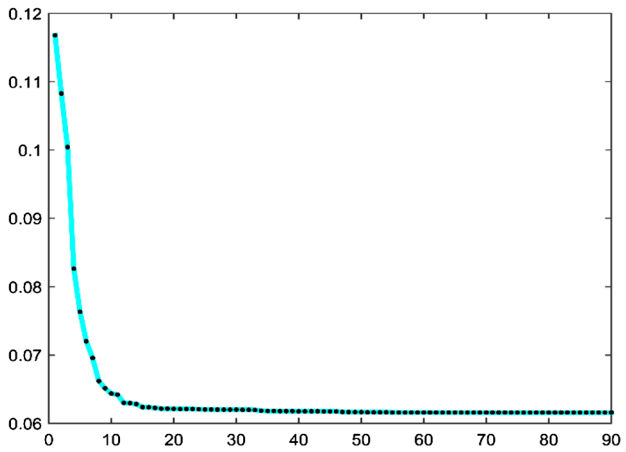

Fig. 19 The diagram of best cost

of wall materials, materials such as copper slag, phospogypsum and fly ash greatly decrease building costs. Moreover, buildings with these materials contribute to more energy-efficient buildings that can be weighted additionally in the Green building approval process. The aim of this paper is to highlight the cost and energy reduction in using alternative construction material. When used as a wall material in buildings, it was obvious that industrial waste brick could greatly reduce the total building cost. Also, using industrial waste materials like copper slag, fly ash and gypsum acts as a supplement to sand and aggregate, thereby highly conserving natural resource.

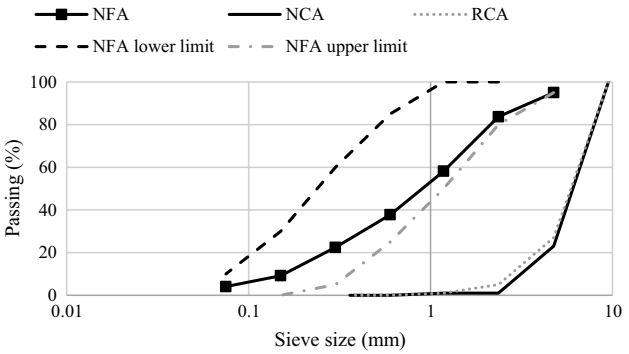

Fig. 20 Stiffness reduction in concrete due to crack opening using conventional materials

In addition, the size variations of the planned industrial bricks minimize cement mortar quantity, labor costs, construction time and ease of plastering due to its smooth surface. Building development, construction processes and maintenance is one of the main concerns in reducing this energy consumption and reducing greenhouse gas emissions. While the energy used in operational construction could be significant, the growing trend to reduced or zero emissions indicates that reducing energy in construction and pre-construction phases of a building life cycle is significance. The embodied energy from building materials and related energies, such as transport, re-usage, recycling and renewables replacement, which should be used with caution, is a key element in energy use during this process. In this case, for measuring the energy and cost optimization, PSO was used. Comparing the RMSE and r-square results have proved PSO as the best model in predicting the strength, energy and cost optimization of construction materials.

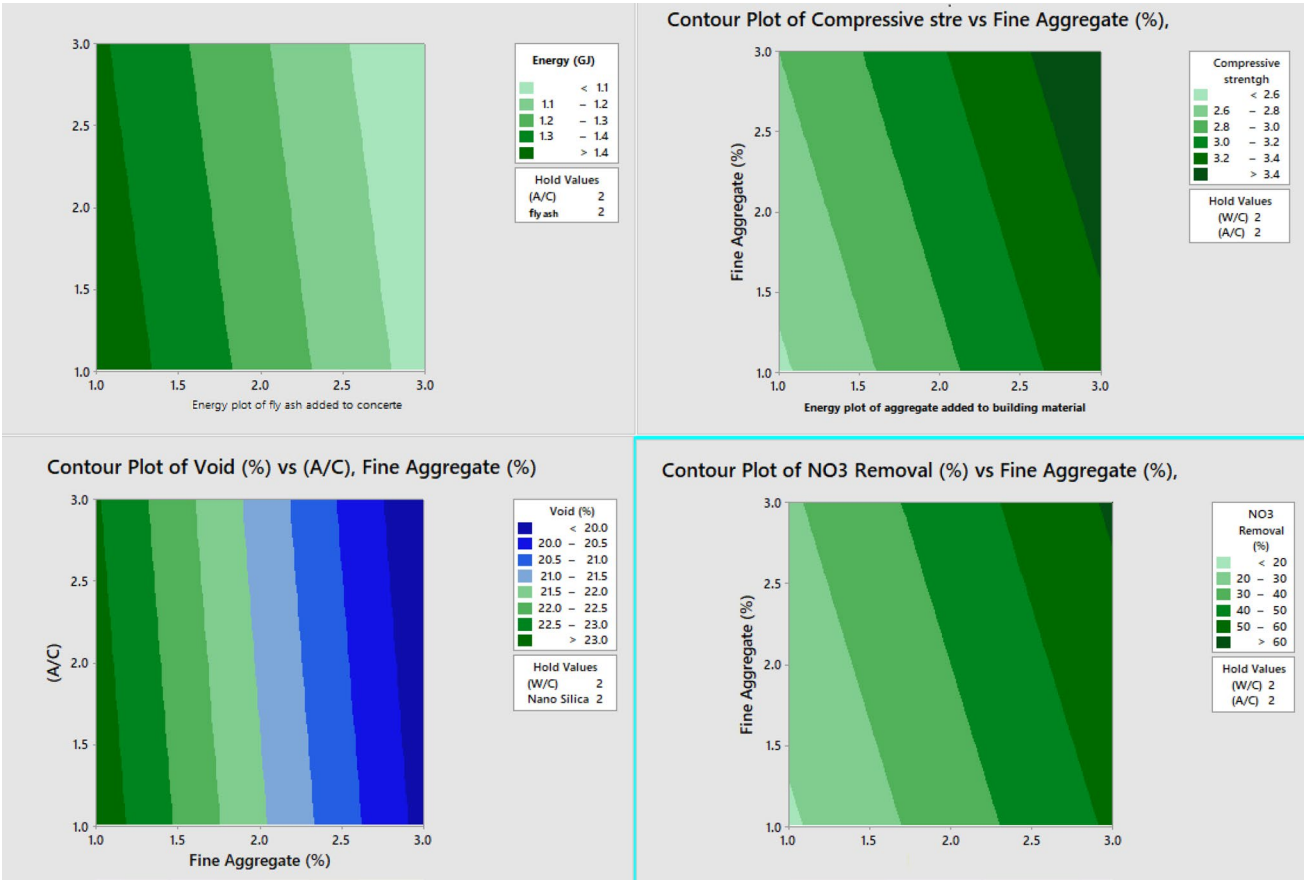

Fig. 21 The energy plot of aggregate added to building material (brick)

References

1. Zuo C, Chen Q, Gu G, Feng S, Feng F, Li R, Shen G (2013) High-speed three-dimensional shape measurement for dynamic scenes using bi-frequency tripolar pulse-width-modulation fringe projection. Opt Lasers Eng 51(8):953–960
2. Huang H, Huang M, Zhang W, Pospisil S, Wu T (2020) Experimental investigation on rehabilitation of corroded RC columns with BSP and HPFL under combined loadings. J Struct Eng 146(8):04020157
3. Zhang C, Gholipour G, Mousavi AA (2020) State-of-the-art review on responses of RC structures subjected to lateral impact loads. Arch Comput Methods Eng. https://doi.org/10.1007/s11831-020-09467-5
4. Zhang C, Wang H (2020) Swing vibration control of suspended structures using the active rotary inertia driver system: theoretical modeling and experimental verification. Struct Control Health Monit 27(6):e2543
5. Alam Z, Sun L, Zhang C, Su Z, Samali B (2020) Experimental and numerical investigation on the complex behaviour of the localised seismic response in a multi-storey plan-asymmetric structure. Struct Infrastruct Eng. https://doi.org/10.1080/15732479.2020.1730914
6. Zhang C, Abedini M, Mehrmashhadi J (2020) Development of pressure-impulse models and residual capacity assessment of RC columns using high fidelity Arbitrary Lagrangian-Eulerian simulation. Eng Struct 224:111219
7. Abedini M, Zhang C (2021) Dynamic vulnerability assessment and damage prediction of RC columns subjected to severe impulsive loading. Struct Eng Mech 77(4):441
8. Zhang C, Mousavi AA (2020) Blast loads induced responses of RC structural members: state-of-the-art review. Compos Part B Eng. https://doi.org/10.1016/j.compositesb.2020.108066
9. Li C, Sun L, Xu Z, Wu X, Liang T, Shi W (2020) Experimental investigation and error analysis of high precision FBG displacement sensor for structural health monitoring. Int J Struct Stab Dyn. https://doi.org/10.1142/S0219455420400118
10. Sun L, Li C, Zhang C, Liang T, Zhao Z (2019) The strain transfer mechanism of fiber bragg grating sensor for extra large strain monitoring. Sensors 19(8):1851
11. Kordestani H, Zhang C, Shadabfar M (2020) Beam damage detection under a moving load using random decrement technique and Savitzky-Golay Filter. Sensors 20(1):243
12. Zheng J, Zhang C, Li A (2020) Experimental investigation on the mechanical properties of curved metallic plate dampers. Appl Sci 10(1):269
13. Jiang D et al (2021) QoE-aware efficient content distribution scheme for satellite-terrestrial networks. In: IEEE transactions on mobile computing. https://doi.org/10.1109/TMC.2021.3074917
14. Abedini M, Zhang C (2020) Blast performance of concrete columns retrofitted with FRP using segment pressure technique. Compos Struct. https://doi.org/10.1016/j.compstruct.2020.113473
15. Yang Y, Yao J, Wang C, Gao Y, Zhang Q, An S, Song W (2015) New pore space characterization method of shale matrix

formation by considering organic and inorganic pores. J Nat Gas Sci Eng 27:496–503
16. Gao N, Tang L, Deng J, Lu K, Hou H, Chen K (2021) Design, fabrication and sound absorption test of composite porous metamaterial with embedding I-plates into porous polyurethane sponge. Appl Acoust 175:107845
17. Gao N, Guo X, Deng J, Cheng B, Hou H (2021) Elastic wave modulation of double-leaf ABH beam embedded mass oscillator. Appl Acoust 173:107694
18. Birkeland J (2002) Design for sustainability: a sourcebook of integrated, eco-logical solutions. Earthscan, London
19. Zhu L, Kong L, Zhang C (2020) Numerical study on hysteretic behaviour of horizontal-connection and energy-dissipation structures developed for prefabricated shear walls. Appl Sci 10(4):1240
20. Zhang C, Li L, Ou J (2010) Swinging motion control of suspended structures: principles and applications. Struct Control Health Monit 17(5):549–562
21. Sun L, Su Z, Xia Y, Zhang C, Li C (2019) Superwide-range fiber bragg grating displacement sensor based on an eccentric gear: principles and experiments. J Aerosp Eng 32(1):04018129
22. Xu H, Zhang C, Li H, Ou J (2014) Real-time hybrid simulation approach for performance validation of structural active control systems: a linear motor actuator based active mass driver case study. Struct Control Health Monit 21(4):574–589
23. Gao N, Lu K (2020) An underwater metamaterial for broadband acoustic absorption at low frequency. Appl Acoust 169:107500
24. Zuo X, Dong M, Gao F, Tian S (2020) The modeling of the electric heating and cooling system of the integrated energy system in the coastal area. J Coast Res 103:1022–1029
25. Hyde R (2000) Climate responsive design: a study of buildings in moderate and hot humid climates. Taylor & Francis
26. Liu J, Liu Y, Wang X (2020) An environmental assessment model of construction and demolition waste based on system dynamics: a case study in Guangzhou. Environ Sci Pollut Res 27(30):37237–37259
27. Liu J, Yi Y, Wang X (2020) Exploring factors influencing construction waste reduction: a structural equation modeling approach. J Clean Prod 276:123185
28. Jiang Q, Shao F, Gao W, Chen Z, Jiang G, Ho Y-S (2018) Unified no-reference quality assessment of singly and multiply distorted stereoscopic images. IEEE Trans Image Process 28(4):1866–1881
29. Xu S, Wang J, Shou W, Ngo T, Sadick A-M, Wang X (2020) Computer vision techniques in construction: a critical review. Arch Comput Methods Eng. https://doi.org/10.1007/s11831-020-09504-3
30. Sun Y, Wang J, Wu J, Shi W, Ji D, Wang X, Zhao X (2020) Constraints hindering the development of high-rise modular buildings. Appl Sci 10(20):7159
31. Wu C, Wu P, Wang J, Jiang R, Chen M, Wang X (2020) Critical review of data-driven decision-making in bridge operation and maintenance. Struct Infrastruct Eng. https://doi.org/10.1080/15732479.2020.1833946
32. Ju Y, Shen T, Wang D (2020) Bonding behavior between reactive powder concrete and normal strength concrete. Constr Build Mater 242:118024
33. Alam Z, Zhang C, Samali B (2020) Influence of seismic incident angle on response uncertainty and structural performance of tall asymmetric structure. Struct Des Tall Spec Build. https://doi.org/10.1002/tal.1750
34. Alam Z, Zhang C, Samali B (2020) The role of viscoelastic damping on retrofitting seismic performance of asymmetric reinforced concrete structures. Earthq Eng Eng Vib 19(1):223–237
35. Zhang C, Alam Z, Sun L, Su Z, Samali B (2019) Fibre Bragg grating sensor-based damage response monitoring of an asymmetric reinforced concrete shear wall structure subjected to progressive seismic loads. Struct Control Health Monit 26(3):e2307
36. Zhu L, Zhang C, Guan X, Uy B, Sun L, Wang B (2018) The multi-axial strength performance of composited structural BCW members subjected to shear forces. Steel Compos Struct 27(1):75–87
37. Gholipour G, Zhang C, Mousavi AA (2020) Numerical analysis of axially loaded RC columns subjected to the combination of impact and blast loads. Eng Struct 219:110924
38. Sun L, Yang Z, Jin Q, Yan W (2020) Effect of axial compression ratio on seismic behavior of GFRP reinforced concrete columns. Int J Struct Stab Dyn. https://doi.org/10.1142/S0219455420400040
39. Zhang W, Tang Z, Yang Y, Wei J (2021) Assessment of FRP–concrete interfacial debonding with coupled mixed-mode cohesive zone model. J Compos Constr 25(2):04021002
40. Yüksek İ (2015) The evaluation of building materials in terms of energy efficiency. Period Polytech Civ Eng 59(1):45–58
41. Zuo C, Li J, Sun J, Fan Y, Zhang J, Lu L, Zhang R, Wang B, Huang L, Chen Q (2020) Transport of intensity equation: a tutorial. Opt Lasers Eng. https://doi.org/10.1016/j.optlaseng.2020.106187
42. Gholipour G, Zhang C, Mousavi AA (2020) Nonlinear numerical analysis and progressive damage assessment of a cable-stayed bridge pier subjected to ship collision. Mar Struct 69:102662
43. Zhang C (2014) Control force characteristics of different control strategies for the wind-excited 76-story benchmark building structure. Adv Struct Eng 17(4):543–559
44. Xu H-B, Zhang C-W, Li H, Tan P, Ou J-P, Zhou F-L (2014) Active mass driver control system for suppressing wind-induced vibration of the Canton Tower. Smart Struct Syst 13(2):281–303
45. Gao N, Wang B, Lu K, Hou H (2021) Complex band structure and evanescent Bloch wave propagation of periodic nested acoustic black hole phononic structure. Appl Acoust 177:107906
46. Liu L, Li J, Yue F, Yan X, Wang F, Bloszies S, Wang Y (2018) Effects of arbuscular mycorrhizal inoculation and biochar amendment on maize growth, cadmium uptake and soil cadmium speciation in Cd-contaminated soil. Chemosphere 194:495–503
47. Hassouneh K, Alshboul A, Al-Salaymeh A (2010) Influence of windows on the energy balance of apartment buildings in Amman. Energy Convers Manag 51(8):1583–1591
48. Dogan E (2004) Turkey's Iran card: energy cooperation in American and Russian vortex. Naval Postgraduate School Monterey
49. Shukla A, Tiwari G, Sodha M (2009) Embodied energy analysis of adobe house. Renew Energy 34(3):755–761
50. Bhatt S (2019) energy efficiency in designing a building: analysis and review. Int J Archit Des Manag 2(1):19–23
51. Esin T (2006) Appropriate material selection for sustainable building. Build Mag 291:83–86
52. Mohsen MS, Akash BA (2001) Some prospects of energy savings in buildings. Energy Convers Manag 42(11):1307–1315
53. Yu Z, Amin SU, Alhussein M, Lv Z (2021) Research on disease prediction based on improved DeepFM and IoMT. In: IEEE Access, vol 9, pp 39043–39054. https://doi.org/10.1109/ACCESS.2021.3062687
54. Kumar A, Buddhi D, Chauhan D (2012) Indexing of building materials with embodied, operational energy and environmental sustainability with reference to green buildings. J Pure Appl Sci Technol 2(1):11–22
55. Li Y, Qiao L, Lv Z (2021) An optimized byzantine fault tolerance algorithm for consortium blockchain. Peer-to-Peer Netw Appl. https://doi.org/10.1007/s12083-021-01103-8
56. Feng W, Lu H, Yao T, Yu Q (2020) Drought characteristics and its elevation dependence in the Qinghai-Tibet plateau during the last half-century. Sci Rep 10(1):1–11

57. Zhang J, Chen Q, Sun J, Tian L, Zuo C (2020) On a universal solution to the transport-of-intensity equation. Opt Lett 45(13):3649–3652
58. Zhang J, Sun J, Chen Q, Zuo C (2020) Resolution analysis in a lens-free on-chip digital holographic microscope. IEEE Trans Comput Imaging 6:697–710
59. Hu Y, Chen Q, Feng S, Zuo C (2020) Microscopic fringe projection profilometry: a review. Opt Lasers Eng. https://doi.org/10.1016/j.optlaseng.2020.106192
60. Abedini M, Mutalib AA, Zhang C, Mehrmashhadi J, Raman SN, Alipour R, Momeni T, Mussa MH (2020) Large deflection behavior effect in reinforced concrete columns exposed to extreme dynamic loads. Front Struct Civ Eng 14(2):532–553
61. Ma L, Liu X, Moradi Z (2021) On the chaotic behavior of graphene-reinforced annular systems under harmonic excitation. Eng Comput. https://doi.org/10.1007/s00366-020-01210-9
62. Zhao Y, Moradi Z, Davoudi M, Zhuang J (2021) Bending and stress responses of the hybrid axisymmetric system via state-space method and 3D-elasticity theory. Eng Comput. https://doi.org/10.1007/s00366-020-01242-1
63. Huang X, Zhu Y, Vafaei P, Moradi Z, Davoudi M (2021) An iterative simulation algorithm for large oscillation of the applicable 2D-electrical system on a complex nonlinear substrate. Eng Comput. https://doi.org/10.1007/s00366-021-01320-y
64. Jiao J, Ghoreishi S-m, Moradi Z, Oslub K (2021) Coupled particle swarm optimization method with genetic algorithm for the static–dynamic performance of the magneto-electro-elastic nanosystem. Eng Comput. https://doi.org/10.1007/s00366-021-01391-x
65. Huang X, Zhang Y, Moradi Z, Shafiei N (2021) Computer simulation via a couple of homotopy perturbation methods and the generalized differential quadrature method for nonlinear vibration of functionally graded non-uniform micro-tube. Eng Comput. https://doi.org/10.1007/s00366-021-01395-7
66. Shariati M, Grayeli M, Shariati A, Naghipour M (2020) Performance of composite frame consisting of steel beams and concrete filled tubes under fire loading. Steel Compos Struct 36(5):587–602
67. Rajaei S, Shoaei P, Shariati M, Ameri F, Musaeei HR, Behforouz B, de Brito J (2021) Rubberized alkali-activated slag mortar reinforced with polypropylene fibres for application in lightweight thermal insulating materials. Constr Build Mater 270:121430
68. Jalali A, Daie M, Nazhadan SVM, Kazemi-Arbat P, Shariati M (2012) Seismic performance of structures with pre-bent strips as a damper. Int J Phys Sci 7(26):4061–4072. https://doi.org/10.5897/IJPS11.1324
69. Arabnejad Khanouki MM, Ramli Sulong NH, Shariati M (2011) Behavior of through beam connections composed of CFSST columns and steel beams by finite element studying. Adv Mater Res 168:2329–2333. https://doi.org/10.4028/www.scientific.net/AMR.168-170.2329
70. Shariati M, Rafie S, Zandi Y, Fooladvand R, Gharehaghaj B, Mehrabi P, Shariat A, Trung NT, Salih MN, Poi-Ngian S (2019) Experimental investigation on the effect of cementitious materials on fresh and mechanical properties of self-consolidating concrete. Adv Concr Constr 8(3):225–237
71. Shariati M, Lagzian M, Maleki S, Shariati A, Trung NT (2020) Evaluation of seismic performance factors for tension-only braced frames. Steel Compos Struct 35(4):599–609. https://doi.org/10.12989/scs.2020.35.4.599
72. Shariati M, Toghroli A, Jalali A, Ibrahim Z (2017) Assessment of stiffened angle shear connector under monotonic and fully reversed cyclic loading. In: Proceedings of the 5th International Conference on Advances in Civil, Structural and Mechanical Engineering-CSM 2017. https://doi.org/10.15224/978-1-63248-132-0-44
73. Shariati M, Mafipour MS, Haido JH, Yousif ST, Toghroli A, Trung NT, Shariati A (2020) Identification of the most influencing parameters on the properties of corroded concrete beams using an adaptive neuro-fuzzy inference system (ANFIS). Steel Compos Struct 34(1):155
74. Zhou Mu, Li Xinyue, Wang Ya, Li Shanshan, Ding Yingyi, Nie Wei (2021) 6G multi-source information fusion based indoor positioning via Gaussian kernel density estimation. IEEE Internet Things J. https://doi.org/10.1109/JIOT.2020.3031639
75. Shariati M, Mafipour MS, Mehrabi P, Ahmadi M, Wakil K, Trung NT, Toghroli A (2020) Prediction of concrete strength in presence of furnace slag and fly ash using Hybrid ANN-GA (Artificial Neural Network-Genetic Algorithm). Smart Struct Syst 25(2):183–195
76. Shariati M, Faegh SS, Mehrabi P, Bahavarnia S, Zandi Y, Masoom DR, Toghroli A, Trung N-T, Salih MN (2019) Numerical study on the structural performance of corrugated low yield point steel plate shear walls with circular openings. Steel Compos Struct 33(4):569–581
77. Shariati M, Mafipour MS, Mehrabi P, Shariati A, Toghroli A, Trung NT, Salih MN (2020) A novel approach to predict shear strength of tilted angle connectors using artificial intelligence techniques. Eng Comput. https://doi.org/10.1007/s00366-019-00930-x
78. Hamidian M, Shariati M, Arabnejad M, Sinaei H (2011) Assessment of high strength and light weight aggregate concrete properties using ultrasonic pulse velocity technique. Int J Phys Sci 6(22):5261–5266
79. Shariati M, Sulong NHR, Khanouki MMA (2010) Experimental and analytical study on channel shear connectors in light weight aggregate concrete. In: Proceedings of the 4th international conference on steel and composite structures, pp 21–23. https://doi.org/10.3850/3978-3981-3808-6218-3853
80. Mohammadhassani M, Akib S, Shariati M, Suhatril M, Arabnejad Khanouki MM (2014) An experimental study on the failure modes of high strength concrete beams with particular references to variation of the tensile reinforcement ratio. Eng Fail Anal 41:73–80. https://doi.org/10.1016/j.engfailanal.2013.08.014
81. Alipour M, Torabi MA, Sareban M, Lashini H, Sadeghi E, Fazaeli A, Habibi M, Hashemi R (2020) Finite element and experimental method for analyzing the effects of martensite morphologies on the formability of DP steels. Mech Based Des Struct Mach 48(5):525–541
82. Ghazanfari A, Assempour A, Habibi M, Hashemi R (2016) Investigation on the effective range of the through thickness shear stress on forming limit diagram using a modified Marciniak-Kuczynski model. Modares Mech Eng 16(1):137–143
83. Ghazanfari A, Soleimani SS, Keshavarzzadeh M, Habibi M, Assempuor A, Hashemi R (2020) Prediction of FLD for sheet metal by considering through-thickness shear stresses. Mech Based Des Struct Mach 48(6):755–772
84. Fazaeli A, Habibi M, Ekrami AA (2016) Experimental and finite element comparison of mechanical properties and formability of dual phase steel and ferrite-pearlite steel with the same chemical composition. Metall Eng 19(2):84–93
85. Qu S, Han Y, Wu Z, Raza H (2020) Consensus modeling with asymmetric cost based on data-driven robust optimization. Group Decis Negot. https://doi.org/10.1007/s10726-020-09707-w
86. Zhang CW, Ou JP, Zhang JQ (2006) Parameter optimization and analysis of a vehicle suspension system controlled by magnetorheological fluid dampers. Struct Control Health Monit 13(5):885–896
87. Abedini M, Zhang C, Mehrmashhadi J, Akhlaghi E (2020) Comparison of ALE, LBE and pressure time history methods

to evaluate extreme loading effects in RC column. Structures. Elsevier, pp 456–466
88. Ma H-J, Yang G-H (2015) Adaptive fault tolerant control of cooperative heterogeneous systems with actuator faults and unreliable interconnections. IEEE Trans Autom Control 61(11):3240–3255
89. Ma H-J, Yang G-H, Chen T (2021) Event-triggered optimal dynamic formation of heterogeneous affine nonlinear multi-agent systems. IEEE Trans Autom Control 66(2):497–512. https://doi.org/10.1109/TAC.2020.2983108
90. Harvey LD (2009) Reducing energy use in the buildings sector: measures, costs, and examples. Energy Eff 2(2):139–163
91. Berge B (2009) The ecology of building materials/translated by C. Butters and F. Henley. Architectural Press Publications, Oxford
92. Venkatarama Reddy B (2009) Sustainable materials for low carbon buildings. Int J Low Carbon Technol 4(3):175–181
93. Huberman N, Pearlmutter D (2008) A life-cycle energy analysis of building materials in the Negev desert. Energy Build 40(5):837–848
94. Stephan A, Crawford RH, De Myttenaere K (2013) A comprehensive assessment of the life cycle energy demand of passive houses. Appl Energy 112:23–34
95. Lv Z, Chen D, Li J (2021) Novel system design and implementation for smart city vertical market. IEEE Commun Magazine. https://doi.org/10.1109/ACCESS.2018.2877023
96. Lou R, Lv Z, Dang S et al (2021) Application of machine learning in ocean data. Multimedia Syst. https://doi.org/10.1007/s00530-020-00733-x
97. Guo Y, Mi H, Habibi M (2021) Electromechanical energy absorption, resonance frequency, and low-velocity impact analysis of the piezoelectric doubly curved system. Mech Syst Signal Process 157:107723
98. Al-Furjan MSH, Dehini R, Paknahad M, Habibi M, Safarpour H (2021) On the nonlinear dynamics of the multi-scale hybrid nanocomposite-reinforced annular plate under hygro-thermal environment. Arch Civ Mech Eng 21(1):4. https://doi.org/10.1007/s43452-020-00151-w
99. Liu H, Shen S, Oslub K, Habibi M, Safarpour H (2021) Amplitude motion and frequency simulation of a composite viscoelastic microsystem within modified couple stress elasticity. Eng Comput. https://doi.org/10.1007/s00366-021-01316-8
100. Yang H, Alphones A, Xiong Z, Niyato D, Zhao J, Wu K (2020) Artificial-intelligence-enabled intelligent 6G networks. IEEE Netw 34(6):272–280. https://doi.org/10.1109/MNET.011.2000195
101. Al-Furjan MSH, Moghadam SA, Dehini R, Shan L, Habibi M, Safarpour H (2020) Vibration control of a smart shell reinforced by graphene nanoplatelets under external load: semi-numerical and finite element modeling. Thin Wall Struct. https://doi.org/10.1016/j.tws.2020.107242
102. Langston C (2015) Green roof evaluation: a holistic 'long life, loose fit, low energy' approach. Constr Econ Build 15(4):76–94
103. Al-Furjan M, Oyarhossein MA, Habibi M, Safarpour H, Jung DW, Tounsi A (2020) On the wave propagation of the multi-scale hybrid nanocomposite doubly curved viscoelastic panel. Compos Struct. https://doi.org/10.1016/j.compstruct.2020.112947
104. Al-Furjan M, Habibi M, won Jung D, Chen G, Safarpour M, Safarpour H (2020) Chaotic responses and nonlinear dynamics of the graphene nanoplatelets reinforced doubly-curved panel. Eur J Mech A Solids 85:104091
105. Al-Furjan M, Oyarhossein MA, Habibi M, Safarpour H, Jung DW (2020) Frequency and critical angular velocity characteristics of rotary laminated cantilever microdisk via two-dimensional analysis. Thin Wall Struct 157:107111
106. Al-Furjan M, Habibi M, Ebrahimi F, Mohammadi K, Safarpour H (2020) Wave dispersion characteristics of high-speed-rotating laminated nanocomposite cylindrical shells based on four continuum mechanics theories. Waves Random Complex Media. https://doi.org/10.1080/17455030.2020.1831099
107. Lv Z, Chen D, Lou R, Alazab A (2021) Artificial intelligence for securing industrial-based cyber–physical systems. Future Gener Comput Syst. 117:291–298. https://doi.org/10.1016/j.future.2020.12.001
108. Lou R, Wang W, Li X, Zheng Y, Lv Z (2021) Prediction of ocean wave height suitable for ship autopilot. IEEE Trans Intell Transp Syst. https://doi.org/10.1109/TITS.2021.3067040
109. Chan Y (2003) Biostatistics 104: correlational analysis. Singap Med J 44(12):614–619
110. Al-Furjan M, Mohammadgholiha M, Alarifi IM, Habibi M, Safarpour H (2020) On the phase velocity simulation of the multi curved viscoelastic system via an exact solution framework. Eng Comput 5:1–17. https://doi.org/10.1007/s00366-020-01152-2
111. Shariati A, Ghabussi A, Habibi M, Safarpour H, Safarpour M, Tounsi A, Safa M (2020) Extremely large oscillation and nonlinear frequency of a multi-scale hybrid disk resting on nonlinear elastic foundation. Thin Wall Struct 154:106840
112. Al-Furjan M, Habibi M, won Jung D, Sadeghi S, Safarpour H, Tounsi A, Chen G (2020) A computational framework for propagated waves in a sandwich doubly curved nanocomposite panel. Eng Comput. https://doi.org/10.1007/s00366-020-01130-8
113. Al-Furjan M, Habibi M, Safarpour H (2020) Vibration control of a smart shell reinforced by graphene nanoplatelets. Int J Appl Mech 12(06):2050066
114. Dixit MK, Culp CH, Fernandez-Solis JL (2014) Calculating primary energy and carbon emission factors for the United States' energy sectors. RSC Adv 4(97):54200–54216
115. Taylor R (1990) Interpretation of the correlation coefficient: a basic review. J Diagn Med Sonogr 6(1):35–39
116. Feng S, Lu H, Tian P, Xue Y, Lu J, Tang M, Feng W (2020) Analysis of microplastics in a remote region of the Tibetan Plateau: implications for natural environmental response to human activities. Sci Total Environ. https://doi.org/10.1016/j.scitotenv.2020.140087
117. Tian P, Lu H, Feng W, Guan Y, Xue Y (2020) Large decrease in streamflow and sediment load of Qinghai-Tibetan Plateau driven by future climate change: a case study in Lhasa River Basin. CATENA 187:104340
118. Lu H, Guan Y, He L, Adhikari H, Pellikka P, Heiskanen J, Maeda E (2020) Patch aggregation trends of the global climate landscape under future global warming scenario. Int J Climatol 40(5):2674–2685
119. Ma H-J, Xu L-X, Yang G-H (2021) Multiple environment integral reinforcement learning-based fault-tolerant control for affine nonlinear systems. IEEE Trans Cybern 51(4):1913–1928. https://doi.org/10.1109/TCYB.2018.2889679
120. Stern DI, Cleveland CJ (2004) Energy and economic growth. Rensselaer Polytechnic Institute. Rensselaer Working Papers in Economics
121. Langston PA, Masling R, Asmar BN (2006) Crowd dynamics discrete element multi-circle model. Safety Sci 44(5):395–417. https://doi.org/10.1016/j.ssci.2005.11.007
122. Dixit MK (2017) Embodied energy and cost of building materials: correlation analysis. Build Res Inf 45(5):508–523
123. Ebrahimi F, Supeni EEB, Habibi M, Safarpour H (2020) Frequency characteristics of a GPL-reinforced composite microdisk coupled with a piezoelectric layer. Eur Phys J Plus 135(2):144
124. Zare R, Najaafi N, Habibi M, Ebrahimi F, Safarpour H (2020) Influence of imperfection on the smart control frequency characteristics of a cylindrical sensor-actuator GPLRC cylindrical shell

using a proportional-derivative smart controller. Smart Struct Syst 26(4):469–480
125. Zhou M, Wang Y, Liu Y, Tian Z (2019) An information-theoretic view of WLAN localization error bound in GPS-denied environment. IEEE Trans Veh Technol 68(4):4089–4093. https://doi.org/10.1109/TVT.2019.2896482
126. Ghabussi A, Ashrafi N, Shavalipour A, Hosseinpour A, Habibi M, Moayedi H, Babaei B, Safarpour H (2019) Free vibration analysis of an electro-elastic GPLRC cylindrical shell surrounded by viscoelastic foundation using modified length-couple stress parameter. Mech Based Des Struct Mach 5:1–25. https://doi.org/10.1080/15397734.2019.1705166
127. Habibi M, Mohammadi A, Safarpour H, Ghadiri M (2019) Effect of porosity on buckling and vibrational characteristics of the imperfect GPLRC composite nanoshell. Mech Based Des Struct Mach. https://doi.org/10.1080/15397734.2019.1701490
128. Habibi M, Mohammadi A, Safarpour H, Shavalipour A, Ghadiri M (2019) Wave propagation analysis of the laminated cylindrical nanoshell coupled with a piezoelectric actuator. Mech Based Des Struct Mach. https://doi.org/10.1080/15397734.2019.1697932
129. Habibi M, Taghdir A, Safarpour H (2019) Stability analysis of an electrically cylindrical nanoshell reinforced with graphene nanoplatelets. Compos Part B Eng 175:107125
130. Ebrahimi F, Habibi M, Safarpour H (2019) On modeling of wave propagation in a thermally affected GNP-reinforced imperfect nanocomposite shell. Eng Comput 35(4):1375–1389
131. Mohammadgholiha M, Shokrgozar A, Habibi M, Safarpour H (2019) Buckling and frequency analysis of the nonlocal strain–stress gradient shell reinforced with graphene nanoplatelets. J Vib Control 25(19–20):2627–2640
132. Safarpour H, Hajilak ZE, Habibi M (2019) A size-dependent exact theory for thermal buckling, free and forced vibration analysis of temperature dependent FG multilayer GPLRC composite nanostructures restring on elastic foundation. Int J Mech Mater Des 15(3):569–583
133. Long Q, Wu C, Wang X (2015) A system of nonsmooth equations solver based upon subgradient method. Appl Math Comput 251:284–299
134. Zhu J, Shi Q, Wu P, Sheng Z, Wang X (2018) Complexity analysis of prefabrication contractors' dynamic price competition in mega projects with different competition strategies. Complexity. https://doi.org/10.1155/2018/5928235
135. Zuo C, Chen Q, Tian L, Waller L, Asundi A (2015) Transport of intensity phase retrieval and computational imaging for partially coherent fields: the phase space perspective. Opt Lasers Eng 71:20–32
136. Zuo C, Sun J, Li J, Zhang J, Asundi A, Chen Q (2017) High-resolution transport-of-intensity quantitative phase microscopy with annular illumination. Sci Rep 7(1):1–22
137. Singh V, Gu N, Wang X (2011) A theoretical framework of a BIM-based multi-disciplinary collaboration platform. Autom Constr 20(2):134–144
138. Zhang C, Ou J (2015) Modeling and dynamical performance of the electromagnetic mass driver system for structural vibration control. Eng Struct 82:93–103
139. Kordestani H, Zhang C (2020) Direct use of the savitzky–golay filter to develop an output-only trend line-based damage detection method. Sensors 20(7):1983
140. Ma H-J, Xu L-x (2020) Decentralized adaptive fault-tolerant control for a class of strong interconnected nonlinear systems via graph theory. IEEE Trans Autom Control. https://doi.org/10.1109/TAC.2020.3014292
141. Xie J, Wen D, Liang L, Jia Y, Gao L, Lei J (2018) Evaluating the validity of current mainstream wearable devices in fitness tracking under various physical activities: comparative study. JMIR Mhealth Uhealth 6(4):e94
142. Qian J, Feng S, Li Y, Tao T, Han J, Chen Q, Zuo C (2020) Single-shot absolute 3D shape measurement with deep-learning-based color fringe projection profilometry. Opt Lett 45(7):1842–1845
143. Abedini M, Zhang C (2020) Performance assessment of concrete and steel material models in LS-DYNA for enhanced numerical simulation, a state of the art review. Arch Comput Methods Eng. https://doi.org/10.1007/s11831-020-09483-5
144. Mousavi AA, Zhang C, Masri SF, Gholipour G (2020) Structural damage localization and quantification based on a CEEMDAN Hilbert transform neural network approach: a model steel truss bridge case study. Sensors 20(5):1271
145. Jiang Q, Wang G, Jin S, Li Y, Wang Y (2013) Predicting human microRNA-disease associations based on support vector machine. Int J Data Min Bioinform 8(3):282–293
146. Mi C, Cao L, Zhang Z, Feng Y, Yao L, Wu Y (2020) A port container code recognition algorithm under natural conditions. J Coast Res 103:822–829
147. Liu J, Wu C, Wu G, Wang X (2015) A novel differential search algorithm and applications for structure design. Appl Math Comput 268:246–269
148. Wu C, Wu P, Wang J, Jiang R, Chen M, Wang X (2021) Ontological knowledge base for concrete bridge rehabilitation project management. Autom Constr 121:103428
149. Schutte JF, Reinbolt JA, Fregly BJ, Haftka RT, George AD (2004) Parallel global optimization with the particle swarm algorithm. Int J Numer Methods Eng 61(13):2296–2315
150. Zhou M, Li Y, Tahir MJ, Geng X, Wang Y, He W (2021) Integrated statistical test of signal distributions and access point contributions for Wi-Fi indoor localization. IEEE Trans Vehi Technol. https://doi.org/10.1109/TVT.2021.3076269